# Novel Wake-up Signaling for Enhanced Energy-Efficiency of 5G and beyond Mobile Devices

# Novel Wake-up Signaling for Enhanced Energy-Efficiency of 5G and beyond Mobile Devices

Soheil Rostami†*, Kari Heiska†, Oleksandr Puchko†, Jukka Talvitie*, Kari Leppanen†, and Mikko Valkama*

†Huawei Technologies Oy (Finland) Co. Ltd, Helsinki R&D Center
*Department of Electronics and Communications Engineering, Tampere University of Technology, Finland
Emails:†{soheil.rostami1, kari.heiska, oleksandr.puchko, kari.leppanen}@huawei.com,
*{soheil.rostami, jukka.talvitie, mikko.e.valkama}@tut.fi

***Abstract*—Low-power and low-latency communication features are vital to extend 5G mobile devices functionalities beyond those of the current networks, and to introduce innovative services and applications. On the other hand, limitations of state-of-the-art cellular modules prevent designing and facilitating such features based on current power saving mechanisms alone. In this paper, a new wake-up signaling for 5G control plane is introduced, aiming to reduce energy consumption of cellular module in downlink. Performance of the proposed scheme in terms of false alarm and misdetection rates are investigated and evaluated. The obtained numerical results show that such a signaling can reduce power consumption of discontinuous reception (DRX) by up to $30\%$, at the cost of negligible increase in signaling overhead.**

***Index Terms*—energy efficiency, mobile device, DRX, wake-up, 5G.**

## I. Introduction

Fifth generation (5G) mobile networks are expected to provide a diverse set of futuristic services such as augmented and virtual reality, cloud gaming and ultra-high-definition video streaming [1]. To satisfy the aggressive requirements of such services, advanced signal processing techniques and high bandwidth - ranging up to $400$ MHz [2] - are imperative. Over the last decade, trend for increased bandwidth has been following the same exponential increase as Moore's Law for semiconductors. However, higher bandwidth communication consumes considerably higher power, and can exhaust the mobile devices battery power very quickly. Due to fact that the battery evolution lags far behind the advances in semiconductor industry, demonstrated by an observation that smartphones' energy density has increased just a few percent during last decade [3], power saving methods are vital to extend 5G mobile devices functionality.

Multiple experimental investigations show that the most energy consuming components of smartphones can be attributed to the cellular module and display [3], [4], [5]. Therefore, designing an energy-efficient cellular module, conserving energy in the battery is extremely paramount, and is the main focus of our work.

This work has received funding from the European Union's Horizon 2020 research and innovation program under the Marie Skłodowska-Curie grant agreement No. 675891 (SCAVENGE), and Tekes TAKE-5 project.

Third generation partnership project (3GPP) has specified DRX, as one of the main solutions for enhanced battery life by means of switching off RF circuitry and other modules for long periods, activating them only for short intervals. In spite of utilizing DRX in long-term evolution (LTE), it is not sufficiently energy efficient, and it still needs to be improved, when very large processing bandwidths are adopted in the future systems.

In the existing literature, the wake-up based schemes have commonly been considered a promising solution for energy-aware sensor nodes. Authors in [6] investigated and summarized the state-of-the-art wake-up receiver hardware and networking protocol proposals. Furthermore, the benefits and challenges of the wake-up scheme, together with the involved trade-offs, were studied. Additionally, authors in [7] designed a high performance low-power digital baseband architecture for wake-up scheme, and the authors analyzed detection performance of the designed architecure in [8], [9].

The concept of passive wake-up scheme is studied in [10], which eliminates the energy supply needed for listening the wake-up signal. The proposed receiver harvests the RF energy from the common signal to power itself up. The proposed scheme can be utilized for IoT and machine to machine communications. More recently, authors in [11], [12] utilized microsleep and DRX to enhance battery life of $5$G mobile devices by enabling 5G mobile device to process only some small pre-grant messages during active times, and consequently to remove empty subframe buffering. The simulation results show that such a scheme can reduce power consumption of mobile device by up to $70\%$.

The main contribution of this paper is to introduce a novel narrow-band control plane signaling, referred to as wake-up signaling (WUS), in order to reduce energy consumption of mobile devices. In the proposed approach, the mobile device monitors WUS at the specific time instants and subcarriers, in order to decide whether to process the actual upcoming

TABLE I
MOST IMPORTANT VARIABLES USED THROUGHOUT THE PAPER.

| Variable | Definition |
|---|---|
| $\text{PW}_{\text{active}}$ | power consumption of cellular module at active state |
| $\text{PW}_{\text{sleep}}$ | power consumption of cellular module at sleep state |
| $t_{su}$ | start-up time of cellular module |
| $t_{pd}$ | power-down time of cellular module |
| $K$ | length of zadoff-chu sequence |
| $M$ | number of mobile devices within PDWCH group |
| $N$ | size of FFT |
| $i[m]$ | wake-up indicator of $m^{th}$ mobile device |
| $\epsilon_i$ | integer carrier frequency offset |
| $s$ | index of OFDM symbol carrying PDWCH |
| $x$ | maximum number of consecutive OFDM symbols within which PDWCH can be located |
| $a$ | maximum number of subcarriers within which integer CFO estimate is sought |
| $\Psi_q$ | PDP of the received signal at $q^{th}$ OFDM symbol |
| $\psi_q$ | discrete periodic correlation function of received signal and complex conjugate of frequency-shifted version of the root zadoff-chu sequence |
| $E_q$ | received energy within the sliding window, belonging to $q^{th}$ OFDM symbol |

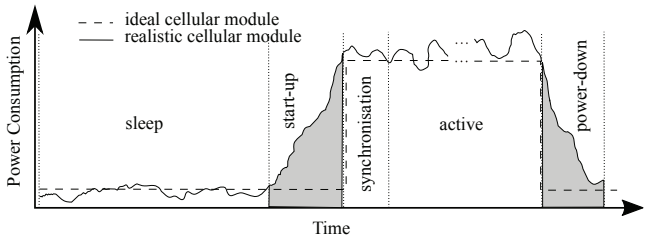


Fig. 1. Ideal and realistic power consumption profiles of cellular module in long DRX. In case of short DRX, start-up and power-down times are shorter, and required power for sleep period is higher. In addition, synchronization stage is not required, since the device is in-synchronization during sleep period of short DRX.

TABLE II
AVERAGE TRANSITIONAL TIME AND REQUIRED POWER CONSUMPTION OF LTE CELLULAR MODULE DURING SHORT AND LONG DRX WHEN CARRIER BANDWIDTH IS 20 MHZ [13].

| DRX Cycle | $\text{PW}_{\text{sleep}}$ | $t_{su}$ | $\text{PW}_{\text{active}}$ | $t_{sync}$ | $t_{pd}$ |
|---|---|---|---|---|---|
| short | 395 mW | 1 ms | 850 mW | 0 ms | 1 ms |
| long | 9.8 mW | 15 ms | 850 mW | 10 ms | 10 ms |

physical downlink control channel (PDCCH) or not. Furthermore, a low-complexity wake-up receiver (WRx) concept is developed to decode the corresponding WUS, and to acquire the necessary time and frequency synchronization.

The rest of this paper is organized as follows. Section II describes the reasons behind energy inefficiency of the baseline DRX mechanism, and proposes wake-up scheme to further improve energy efficiency of cellular module. WUS structure and its detection procedure are described and discussed in Section III. These are followed by simulation results and conclusion in Sections IV and V, respectively.

For readers' convenience, the most essential variables used throughout the paper are listed in Table I.

## II. PROBLEM DESCRIPTION AND PROPOSED WAKE-UP SCHEME

### A. DRX and Power Consumption Challenges

Ideally, cellular module is expected to transit from sleep to active state or vice versa sharply, as illustrated in dashed line in Fig. 1. However, because of hardware preparation time, cellular module power consumption shape changes from purely ideal rectangular to a smooth contour without sharp edges as shown in solid line in Fig. 1. As a result, considerable amount of energy is wasted during start-up and power-down times during a DRX cycle, as depicted in gray areas in Fig. 1. The slightly smoothened power consumption profile then also translates into shorter sleep time, compared to the ideal scenario, consequently reducing sleep ratio and increasing energy consumption of DRX.

As a concrete example, Table II expresses the average transitional timings and power consumption states of both short and long DRX cycles based on measurements of multiple different LTE cellular modules [13]. As can be seen, for short DRX cycle, sleep power consumption ($\text{PW}_{\text{sleep}}$) is much higher than for long DRX cycle. This, in turn, has a direct influence on start-up time ($t_{su}$) and power-down time ($t_{pd}$). In case of short DRX, due to fact that baseband unit (BBU) is ON during sleep period, $t_{su}$ and $t_{pd}$ are shorter than in long DRX. In short-DRX cycle, time required for synchronization $t_{sync}$ is negligible. Required power for active state ($\text{PW}_{\text{active}}$), besides of implementation, varies based on bandwidth and other communication parameters.

In respect to latency requirements, it is beneficial to process PDCCH in a very short DRX cycle to receive uplink (UL) grants or downlink (DL) data traffic, and promptly make an appropriate reaction. However, decoding the PDCCH requires a fast Fourier transform (FFT) whose size depends on the carrier bandwidth, and employs a blind decoding approach, where it hypothesizes over 44 different options of PDCCH locations [14], [15]. Especially for higher bandwidth carriers, the PDCCH rendering is very computationally intensive and power consuming. Therefore, decoding PDCCH frequently reduces the advantages of DRX, and high power consumption overhead is inevitable.

It has been shown in [16] that the time period for which mobile device monitors channel without any data allocation has a major impact on battery consumption. For instance, according to the experimental results, video streaming and web browsing traffic as two key 5G use cases have empty PDCCH for 25% and 40% of time, respectively. Furthermore, this problem is severe in unsaturated traffic scenarios, where many of the DRX cycles have no data allocation for a particular mobile device. Therefore, reducing energy consumption of empty DRX cycles, has a significant potential to expand the battery life time of mobile devices.

### B. Proposed Wake-up Scheme

In the proposed mechanism, the mobile device is configured with wake-up signaling and WRx processing in order to save battery life time, suitable for enhanced mobile broadband and massive machine type communication, which have small amounts of data at short intervals. In every wake-up cycle (w-cycle), WRx monitors physical downlink wake-up channel (PDWCH) for a specific on-duration time to determine if any data is scheduled or not. Occasionally, based on the interrupt signal from WRx, the BBU switches on, decodes both PDCCH and physical downlink shared channel (PDSCH), and performs connected-mode procedures.

The WUS per each WRx is represented by 1-bit data, referred to as wake-up indicator (WI), where 0 indicates WRx to not wake up BBU and 1 represents WRx to wake up BBU because there is a packet to receive. Each WI is uniquely code multiplexed to selected time-frequency resources, as described in Section III. When WI of 1 is sent to WRx, network expects the corresponding mobile device to decode the PDCCH with time offset of $t_{of}$. In other words, PDWCH indirectly informs WRx of potential scheduling on PDCCH with time offset of $t_{of}$ or rather if it can skip interrupting BBU for the rest of the w-cycle. Fig. 2 depicts the operation and power consumption of the proposed cellular module with WRx and conventional DRX-enabled cellular module.

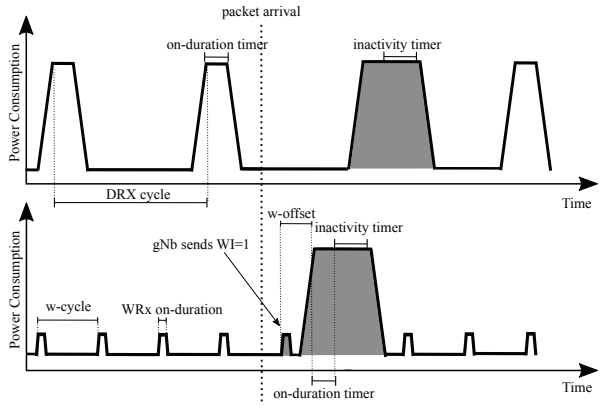


Fig. 2. Power consumption profiles of typical DRX mechanism and the proposed WRx-enabled cellular module.

BBU, after receiving PDCCH message at active state for on-time duration, initiates its inactivity timer. After the inactivity timer is initiated, if a new PDCCH message is received before the expiration of inactivity timer, BBU re-initiates its inactivity timer. However, if there is no PDCCH message received before expiration of the inactivity timer, a sleep period starts, and the WRx-enabled cellular module switches to its sleep state, and WRx operates according to its w-cycle.

The introduction of PDWCH has two fundamental consequences, misdetection and false alarm. In latter case, WRx wakes up in a predefined time instant, and wrongly identifies 0 as 1 for WI, leading to unnecessary power consumption of BBU, thus the false alarm rate is required to be minimized. The former is corresponding to the case where WI of 1 is sent, but WRx decodes it as 0 incorrectly. Such misdetection can add an extra delay, and waste capacity in both PDCCH and PDSCH. Therefore, the probability of misdetection ($P_{md}$) requirement of PDWCH is eventually stricter than probability of false alarm ($P_{fa}$). Simulation results in Section IV, verify that the proposed scheme, building on the signaling structure and decoder principle described in Section III, can achieve very low $P_{md}$ and $P_{fa}$ for SNRs larger than 0 dB.

## III. Wake-up Signaling Structure and Receiver Processing

### A. Signaling Structure

The proposed signaling is based on 5G base station (gNB) transmitting set of Zadoff-Chu (ZC) signatures with different cyclic shifts over a set of dedicated and pre-reported subcarriers, carrying set of WIs along with synchronization. A pool of known cyclic shift sequences is allocated to each gNB within a cell with a cell-specific root index, providing low inter-cell interference.

The ZC sequences have ideal cyclic auto-correlation, which is important for obtaining an accurate timing estimation and WRx identification. Additionally, the cross-correlation between different sequences based on cyclic shifts of the same ZC root sequence is zero at the WRx as long as the cyclic shift used when generating the sequences is larger than the maximum round-trip propagation time in the cell plus the maximum delay spread of the channel [17]. Root ZC sequence ($z^r[n]$) is a polyphase exponential ZC sequence with root index of $r$, and can be formulated as

$$z^r[n] = \exp\left\{-j\frac{\pi r n(n+1)}{K}\right\} \text{ for } n \in \{0, ..., K-1\}, \quad (1)$$

where $K$ refers to the length of sequences, assumed odd, and needs to be integer larger than and relatively prime with respect to $r$ [18]. An odd-length ZC sequence is symmetric to its center element, and enables design of hardware-efficient architectures for its generation. Further, if $K$ is prime, the discrete Fourier transform (DFT) of $z^r[n]$ is another ZC sequence ($Z^r[k]$). For sake of readability, root index notation is omitted for the rest of the paper.

PDWCH is transmitted within the first symbol of subframe corresponding to the w-cycle. The main reason for transmitting PDWCH in the first symbol is to provide adequate time ($\leq t_{of}$) for WRx to possibly switch on BBU as early as possible. Therefore, BBU can prepare to decode PDCCH, and eventually, demodulate and decode PDSCH. This reduces the processing delay, and thus the overall DL transmission delay.

The multiple WIs are code multiplexed to a set of subcarriers which enables efficient usage of radio resource elements, and reduces the power consumption of WRx. We refer to a set of WIs transmitted on the same set of subcarriers as a PDWCH group.

We consider a multi-user single-cell scenario, where each sequence within PDWCH group is chosen from a set of $M$ cyclic-shifted ZC sequences with length of $K$. Furthermore, during first OFDM symbol of predefined subframe, $K$ contiguous subcarriers are utilized while the exact location of

PDWCH is indicated by the frequency offset parameter. For simplicity, we assume that subcarriers with relative indices to the DC subcarrier $k \in \{0, ..., K-1\}$ are used for PDWCH. Therefore, DFT of PDWCH group signal for $M$ mobile devices is

$$Y[k] = Z_0 + \sum_{m=1}^{M} i[m] Z_m, \tag{2}$$

where

$$Z_m = Z[k] \text{exp}\left\{-j\frac{2\pi\tau[m]}{K}\right\}, \tag{3}$$

and $i[m]$ for $m \in \{1, ..., M\}$ is a binary variable, representing WI of $m^{th}$ mobile device with its unique cyclic shift of $\tau[m] = mK_{cs}$, where $M \leq \lfloor K/K_{cs} \rfloor - 1$. $Z_0$ is always transmitted within PDWCH group, helping WRx to retain synchronization even if $i[m] = 0,\ \forall m \in \{1, ..., M\}$. In Eq. (3) and in the rest of the paper, modulo-$K$ indexing is assumed. The simplified PDWCH signal structure is illustrated in Fig. 3.

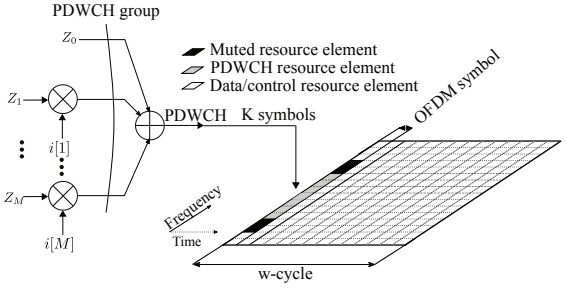


Fig. 3. Time-frequency grid illustrating PDWCH signal structure, $Z_m$ refers to root ZC sequence with cyclic-shift of $\tau[m]$.

### *B. Receiver Processing*

In the proposed scheme, high-power high-precision oscillator is assumed to be kept ON, therefore implications of clock drift are negligible during short w-cycles. In order to further reduce impact of any clock drift, the proposed receiver has two-stage mechanism to recover any potential symbol time offset (STO) and carrier frequency offset (CFO). At the first stage, which is performed in pre-FFT domain (time domain), maximum likelihood-estimator is applied to identify STO ($\delta$) and fractional CFO ($\epsilon_f$). After the synchronization of the symbol timing, cyclic prefix (CP) is removed correspondingly, and the second stage is performed in FFT domain. In this work, we mainly focus on the second stage, while the first stage is not specifically addressed (readers may refer to [19]).

Assuming that the initial synchronization provides an adequate orthogonality between subcarriers, $N$-point FFT output of $q^{th}$ OFDM symbol is represented as $\mathbf{R}_q = [R_q[1], ..., R_q[K]]^T$. Under the assumption that $s$ is the index of OFDM symbol carrying PDWCH, $R_s[k]$ can be written as

$$R_s[k] = Y[k-\epsilon_i] H[k-\epsilon_i] \text{exp}\left\{-j\frac{2\pi\upsilon(k-\epsilon_i)}{N}\right\} + W[k], \tag{4}$$

where $\upsilon$ denotes residual timing error, normalized by the sampling period, $H[k]$ is the channel frequency response at the $k^{th}$ subcarrier, $\epsilon_i$ refers to the integer CFO, and $W[k]$ is a circularly-symmetric white Gaussian noise process with average power $\sigma_w^2$. Without loss of generality and for notational simplifications, we assume $\upsilon$ is incorporated into $H[k]$, therefore in the following, $\text{exp}\left\{-j\frac{2\pi\upsilon k}{N}\right\}$ from Eq. (4) is removed and absorbed as part of $H[k]$. Due to ambiguity of the arrival time of OFDM symbol carrying PDWCH, WRx requires to observe a consecutive set of $x$ statistically independent FFT outputs $\mathcal{R} = [\mathbf{R}_1, ..., \mathbf{R}_x]$, in order to locate the PDWCH symbol.

In general, at the second stage, the WRx needs to perform three tasks, 1) to acquire the position of PDWCH symbol ($s$), 2) to receive its WI ($i[m]$), and 3) to obtain integer CFO ($\epsilon_i$). In the following, we introduce an estimation method of unknown parameters $(\hat{s}, \hat{i}[m], \hat{\epsilon}_i)$.

In the proposed approach, WRx benefits from ideal cyclic auto- and cross-correlation properties of ZC sequences by computing received signal's power delay profile (PDP) through a frequency-domain matched filter. For this purpose, the absolute square of the correlation of the received $q^{th}$ OFDM symbol with cyclic- and phase-shifted root ZC sequences is utilized and can be expressed as

$$\Psi_q(l, \epsilon_i) = \left| \sum_{n=0}^{K-1} r_q[n] z^*[n+l] \text{exp}\left\{ j\frac{2\pi\epsilon_i}{K}(n+l) \right\} \right|^2, \tag{5}$$

where $r_q[n]$ is the time-domain sequence corresponding to $R_q[k]$. As it can be seen from Eq. (5), the $\Psi_q(l, \epsilon_i)$ is at maximum on the correctly estimated CFO and PDWCH symbol. In order to reduce the implementation complexity, a hybrid time/frequency domain method is considered for the second stage. Using the properties of FFT, $\Psi_q(l, \epsilon_i)$ can be computed as

$$\Psi_q(l, \epsilon_i) = |\psi_q(l, \epsilon_i)|^2 = \left| \text{IFFT}\left\{ R_q[k] Z^*[k-\epsilon_i] \right\}_l \right|^2, \tag{6}$$

where $\psi_q(l, \epsilon_i)$ is the discrete periodic correlation function at lag $l$ of received signal and complex conjugate of frequency-shifted version of the root ZC sequence.

For clarity, after removing CP at the first stage, and obtaining initial synchronization, $r_q[n]$ is translated to the frequency domain using $N$-point FFT, as shown in Fig. 4. Those $K$ subcarriers corresponding to PDWCH are extracted from the output of the FFT using subcarrier demapper. The result of subcarrier demapping ($R_q[k]$) is multiplied by the complex-conjugate root ZC sequences with potential frequency offsets ($Z^*[k-\epsilon_i]$), and the result of each is oversampled - by factor of $L = 2^N/K$, where $N$ is IFFT size - by padding zeros in order to balance between detection performance and implementation complexity. Next, the IFFT block, transforms the product of $R_q[k]$ and $Z^*[k-\epsilon_i]$ from frequency into time domain. And then, PDP samples are calculated by squaring the absolute value of the time-domain data ($\psi_q(l, \epsilon_i)$). The received energy within the sliding window corresponding to

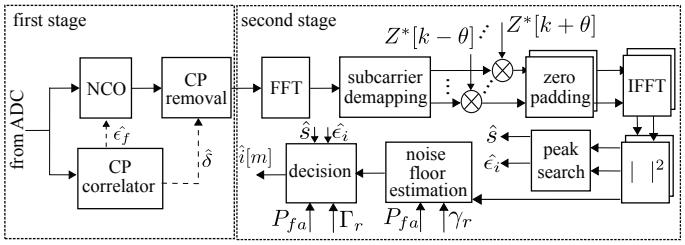


Fig. 4. Block diagram of main components of WRx.

$m^{th}$ interval $m \in \{0, ..., M\}$, belonging to $q^{th}$ OFDM symbol can be written as

$$E_q(m, \epsilon_i) = \sum_{l=mLK_{cs}}^{(m+1)LK_{cs}-1} \Psi_q(l, \epsilon_i). \tag{7}$$

### C. Detection and Thresholds

Under the assumption that the $LK_{cs}$ samples in the sliding window in the absence of WI are uncorrelated Gaussian noise with variance $\sigma_w^2$, the samples of $\psi(l, \epsilon_i)$ also present Gaussian distribution with zero mean and variance of $K\sigma_w^2$. Consequently, $\Psi(l, \epsilon_i)$ has a central Chi-squared distribution with 2 degrees of freedom with noise floor of $\beta = K\sigma_w^2$. Therefore, the absolute WI detection threshold ($\Gamma$) can be calculated under the hypothesis of WI$= 0$ within a given $P_{fa}$, as

$$P_{fa} = 1 - F_1(\Gamma)^{LK_{cs}}, \tag{8}$$

where $F_1(\Gamma)$ is the cumulative distribution function (CDF) of $\Gamma$. Without loss of generality, we can assume that $\Gamma = \beta\Gamma_r$, where $\Gamma_r$ is the threshold relative to the noise floor $\beta$. By doing such, dependency of $F_1(\Gamma_r)$ on the noise variance is removed, and can be modeled as a central Chi-squared random variable with $2LK_{cs}$ degrees of freedom [20] expressed as

$$F_1(\Gamma_r) = 1 - \exp\{-\Gamma_r\} \sum_{k=0}^{LK_{cs}-1} \frac{1}{k!}{\Gamma_r}^k, \tag{9}$$

where $\Gamma_r$ is a pre-computed coefficient, and stored in memory.

Similarly, the noise power samples at the input to noise floor estimation follows a central Chi-square distribution with 2 degrees of freedom, expressed as

$$F_2(\Upsilon_r) = 1 - \exp\{-\Upsilon_r\}. \tag{10}$$

In above, $\Upsilon_r$ is the relative detection threshold for noise floor estimation, and is set as follows

$$P_{fa} = 1 - F_2(\Upsilon_r), \tag{11}$$

while the absolute noise floor threshold ($\Upsilon$) can be computed as

$$\Upsilon = \frac{F_2^{-1}(1 - P_{fa})}{N} \sum_{l=1}^{N} \Psi_q(l, \epsilon_i), \tag{12}$$

where $F_2^{-1}$ is the inverse of CDF of $F_2$. Finally, $\beta$ can be estimated as [21]

$$\beta = \frac{1}{N_s} \sum_{\substack{l=1 \\ \Psi_q(l,\epsilon_i)<\Upsilon}}^{N} \Psi_q(l, \epsilon_i), \tag{13}$$

where the accumulation is over all samples less than $\Upsilon$, and $N_s$ is the number of available samples.

Once the PDP samples of all potential frequency offsets of the root ZC sequence are obtained, $E_q(0, \epsilon_i)$ per frequency offset per OFDM symbol are calculated, and the corresponding frequency offset and index of OFDM symbol of the maximum of received energy are chosen as estimates of $\epsilon_i$ and $s$, respectively.

Again by utilizing sliding window, if the received energy of estimated OFDM symbol in $m^{th}$ interval ($E_{\hat{s}}(m, \hat{\epsilon}_i)$) exceeds absolute WI detection threshold ($\Gamma$), $m^{th}$ WRx decodes $\hat{i}[m] = 1$, otherwise $\hat{i}[m] = 0$. Briefly, initially $(\hat{s}, \hat{\epsilon}_i)$ is obtained as follows

$$(\hat{s}, \hat{\epsilon}_i) = \underset{(s,\epsilon_i)\in\Theta}{\operatorname{argmax}}\{E_s(0, \epsilon_i))\} \tag{14}$$

and then

$$\hat{i}[m] = \begin{cases} 0, & \text{for } E_{\hat{s}}(m, \hat{\epsilon}_i) < \Gamma \\ 1, & \text{for } E_{\hat{s}}(m, \hat{\epsilon}_i) \geq \Gamma \end{cases} \tag{15}$$

under the assumption that $(s, \epsilon_i)$ is restricted to a given parameter space $\Theta$. As it can be seen, accurate realization of the parameter estimator in Eq. (14) requires a search over $x \times a$ values where $x$ denotes the number of considered FFT outputs and $a$ refers to the maximum span of subcarriers for which the integer CFO estimate is sought. For example, assuming that the integer CFO can be a maximum of $\pm 2$ subcarriers, then $a = 5$.

Because of very simple hardware architecture of WRx, start-up and power-down time durations for WRx are extremely short. The processing requires a few OFDM symbols and a few subcarriers in each w-cycle, in contrast to DRX, where BBU needs to operate full bandwidth for multiple symbols. In other words, narrowband reception of wake-up signaling requires less signal processing, consequently needing also less memory and operations. Moreover, its narrowband signal structure has improved sensitivity due to its low in-band receive noise.

In this work, power consumption of the realization of architecture for the WRx by integrating the processing to an available LTE-optimized 16 nm CMOS-based RFIC is estimated. According to the pre-design estimation, the processing consumes only up 57 mW power, including its radio and digital processing, when $K = 117$ and $N = 128$, regardless of carrier bandwidth. Its required clock can be shared from the main BBU of cellular module.

## IV. Simulation Results and Analysis

In the numerical evaluations, we consider 5G frame structure, where transmission over the subcarriers is arranged into

radio frames of 10 ms long, each of which is divided into ten equally sized individual subframes, where each subframe is consisting of 14 consecutive OFDM symbols while the subcarrier spacing is assumed to be 15 kHz. Additionally, within each frame, primary and secondary synchronization signals are utilized for network synchronization. Further, for channel modeling purposes, we adopt the extended pedestrian A model (EPA) developed by 3GPP [22], for the performance analysis and comparison. It is assumed that the carrier bandwidth is 20 MHz.

For traffic modeling purposes, the ETSI model [23] is applied, which is widely used in various analytical and simulation studies of 3GPP mobile radio networks. In the employed traffic model, a packet service session contains one or several packet calls with exponentially distributed session inter-arrival time with mean of 200 ms. Each packet call itself consists of a sequence of packets with exponentially distributed packet inter-arrival time, with mean of 10 ms. The mean session rate is one session per minute.

In our simulations, we focus on a single cell and single PDWCH group. Furthermore, each simulation scenario lasts for $100,000$ frames, and is repeated $10,000$ times for averaging results. Each PDWCH group has $M = 7$ users (moving at a walking speed of 3 km/h), utilizing ZC sequences with length of $K = 117$ and root index of $r = 31$. We also assume $x = 3$, $a = 5$, and $K_{cs} = 13$. Finally, inactivity timer, on-time duration and offset time are considered to be 12 ms, 1 ms and 15 ms, respectively.

Fig. 5 shows a receiver operating characteristic (ROC) curve of the proposed wake-up scheme under EPA channel model at three different SNR values. As it can be expected, for all three ROC curves, there is a trade-off between $P_{md}$ and $P_{fa}$. Furthermore, by comparing the ROC curves at different SNRs, we note that the $P_{md}$ at SNR=-10 dB with $P_{fa} = 10\%$ is higher than that for SNR=-7 dB and SNR=-4 dB by 37% and 69%, respectively. As it can seen, for higher SNRs, ROC becomes closer and closer to an ideal curve.

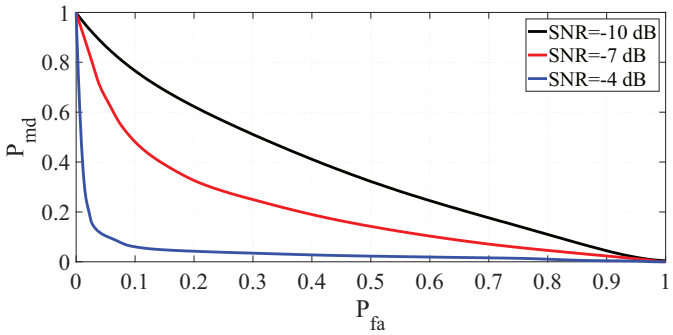


Fig. 5. ROC curves for three different SNRs.

The simulation results of $P_{md}$ for varying SNR with constant false alarm rates are indicated in Fig. 6. Similar to Fig. 5, for better SNR environments ($\geq$-2 dB), $P_{md}$ reduces drastically. The misdetection rate for lower false alarm rate at a given SNR is higher than the corresponding misdetection rate of higher false alarm rate. This implies the need for configuring the target false alarm rate individually for different use cases based on their energy and delay requirements.

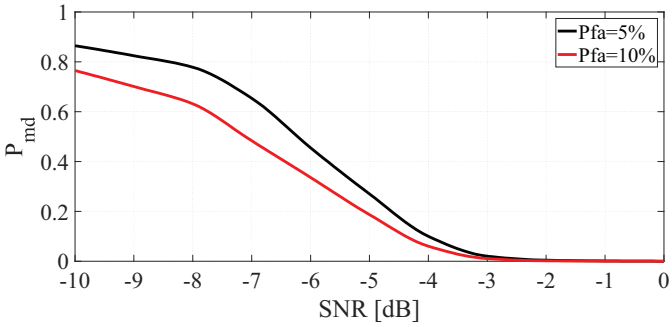


Fig. 6. Misdetection rate as a function of SNR, at fixed false alarm rates.

Moreover, Fig. 7 and Fig. 8 illustrate synchronization failure rate ($P_{sf}$) and mean squared error (MSE) of the CFO estimate as a function of SNR, respectively. As it can be expected, the failure rate reduces for higher SNR. Interestingly, the synchronization failure rate is not dependent on $P_{fa}$. The main reason for such a trend is because of estimating $\epsilon_i$ without utilizing threshold (which is fixed based on target false alarm rate). Synchronization failure impacts directly the WI detection rate, and that is the main reason to try to reduce it as small as possible.

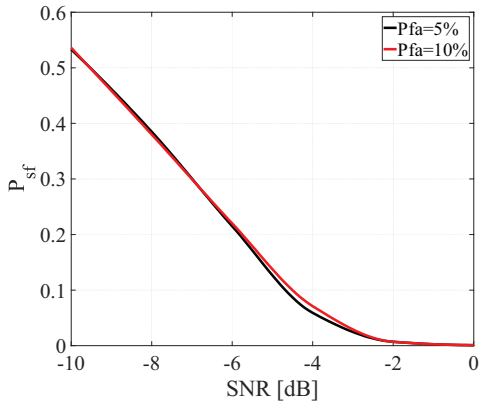


Fig. 7. Synchronization failure rate as function of SNR under different constant false alarm rates.

Moreover, because of utilizing PDP values for selecting a PDWCH symbol, the probability of detection of the correct PDWCH OFDM symbol is almost 100%, even for low SNR values in the order of -10 dB. The PDPs of other OFDM symbols are extremely low compared to that of the PDWCH symbol. It is very vital to have high PDWCH detection probability, since misdetection of PDWCH symbol can increase both false alarm and misdetection of WI directly.

Finally, the energy saving performance of WRx-enabled and DRX-enabled cellular modules, for different values of w-cycle and short/long DRX cycle length are compared. In addition, for fair comparison, we assume that DRX long cycle

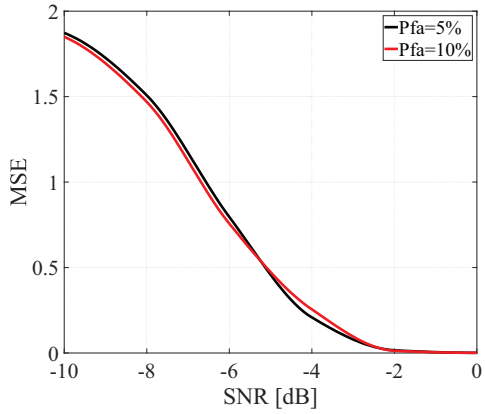


Fig. 8. MSE of $\epsilon_i$ normalized by subcarrier spacing as function of SNR under different constant false alarm rates.

TABLE III
ACHIEVED VALUES OF POWER CONSUMPTION OF CELLULAR MODULE WITH WRX AND DRX, ASSUMING THAT $P_{fa} = 0.1$ AND $P_{md} = 0.01$.

| Delay | 10 ms | 20 ms | 30 ms | 40 ms | 50 ms |
|---|---|---|---|---|---|
| WRx | 211.6 mW | 110.2 mW | 94.86 mW | 89.92 mW | 87.72 mW |
| DRX | 218.6 mW | 158.8 mW | 127.2 mW | 109.6 mW | 98.93 mW |

is four times of its short DRX cycle, and also that the short DRX timer is 16. Table III shows the resulting average delay and power consumption values for aforementioned traffic model.

For tighter delay constraint, both methods consume higher amounts of energy, the main reason being that cellular module remains in active state more than in case with longer delay constraints. As it can be seen from Table III, for the same delay requirements, cellular module with WRx consumes much less power than DRX. For instance, if buffering delay constraint is 20 ms, by utilizing DRX, mobile device may achieve average power consumption of 158.8 mW, while with employing WRx, this can be reduced to 110.2 mW. However, power consumption of WRx approaches that of DRX for very large or very short delays. This is primarily because of consuming higher amount of energy in sleep state in WRx than the deep sleep of long DRX cycle, and also due to overhead of start-up and power-down in very short w-cycles.

## V. CONCLUSION

In this paper, a novel wake-up scheme was proposed together with an efficient wake-up signaling structure, such that reliable WUS detection, and thus large energy savings can be obtained in 5G and beyond mobile devices. Efficient receiver processing solutions, building on the proposed wake-up signal structure, were also described, for synchronization and wake-up symbol location estimation purposes, as well as to decode the actual wake-up indicator bit. Numerical evaluations building on the ETSI traffic model were also provided and analyzed, demonstrating reliable system operation even at very low SNRs. Finally, it was shown that up to 30% reduction in the mobile device power consumption can be obtained, compared to existing DRX solutions.

## REFERENCES


[1] F. Boccardi, R. W. Heath, A. Lozano, T. L. Marzetta, and P. Popovski, "Five disruptive technology directions for 5G," *IEEE Communications Magazine*, vol. 52, no. 2, pp. 74–80, February 2014.

[2] S. Parkvall, E. Dahlman, A. Furuskar, and M. Frenne, "NR: The new 5G radio access technology," *IEEE Communications Standards Magazine*, vol. 1, no. 4, pp. 24–30, Dec 2017.

[3] M. Lauridsen, P. Mogensen, and T. B. Sorensen, "Estimation of a 10 Gb/s 5G receiver's performance and power evolution towards 2030," in *Proc. IEEE VTC 2005 Fall*, Sept 2015, pp. 1–5.

[4] "Designing mobile devices for low power and thermal efficiency," Qualcomm Technologies, Inc., Tech. Rep., Oct. 2013.

[5] A. Carroll and G. Heiser, "An analysis of power consumption in a smartphone," in *Proc. USENIXATC2010*. Berkeley, CA, USA: USENIX Association, 2010, pp. 21–21.

[6] I. Demirkol, C. Ersoy, and E. Onur, "Wake-up receivers for wireless sensor networks: benefits and challenges," *IEEE Wireless Communications*, vol. 16, no. 4, pp. 88–96, Aug 2009.

[7] N. S. Mazloum, J. N. Rodrigues, O. Andersson, A. Nejdel, and O. Edfors, "Improving practical sensitivity of energy optimized wake-up receivers: Proof of concept in 65-nm cmos," *IEEE Sensors Journal*, vol. 16, no. 22, pp. 8158–8166, Nov 2016.

[8] N. S. Mazloum, J. N. Rodrigues, and O. Edfors, "Sub-VT design of a wake-up receiver back-end in 65 nm CMOS," in *Proc. IEEE SubVT 2012*, Oct 2012, pp. 1–3.

[9] N. S. Mazloum and O. Edfors, "Performance analysis and energy optimization of wake-up receiver schemes for wireless low-power applications," *IEEE Transactions on Wireless Communications*, vol. 13, no. 12, pp. 7050–7061, Dec 2014.

[10] S. Rostami, K. Heiska, O. Puchko, K. Leppanen, and M. Valkama, "Wireless powered wake-up receiver for Ultra-Low-Power devices," in *Proc. IEEE WCNC 2018 - SSW*, Barcelona, Spain, Apr. 2018.

[11] M. Lauridsen, "Studies on mobile terminal energy consumption for LTE and future 5G," Ph.D. dissertation, Aalborg University, Jan. 2015.

[12] S. Rostami, K. Heiska, O. Puchko, K. Leppanen, and M. Valkama, "Robust Pre-Grant signaling for Energy-Efficient 5G and beyond mobile devices," in *Proc. IEEE ICC'18 GCSN*, Kansas City, USA, May 2018.

[13] M. Lauridsen, L. Noel, T. Sorensen, and P. Mogensen, "An empirical LTE smartphone power model with a view to energy efficiency evolution," *Intel Technology Journal*, vol. 18, no. 1, pp. 172–193, 3 2014.

[14] "Evolved universal terrestrial radio access (E-UTRA); physical layer procedures," 3GPP, TS 36.213, Tech. Rep., Mar. 2014.

[15] "Evolved universal terrestrial radio access (E-UTRA); user equipment (UE) procedures in idle mode," 3GPP, TS 36.304, Tech. Rep., Jan. 2016.

[16] "UE power consideration based on days-of-use," Qualcomm Incorporated, R1-166368, Tech. Rep., Aug. 2016.

[17] S. P. Erik Dahlman and J. Skold, *4G LTE/LTE-Advanced for Mobile Broadband*. Academic Press, 2011.

[18] J. C. Guey, "The design and detection of signature sequences in time-frequency selective channel," in *Proc. IEEE PIMRC 2008*, Sept 2008, pp. 1–5.

[19] J. J. van de Beek, M. Sandell, and P. O. Borjesson, "ML estimation of time and frequency offset in OFDM systems," *IEEE Transactions on Signal Processing*, vol. 45, no. 7, pp. 1800–1805, Jul 1997.

[20] J. G. Proakis and D. K. Manolakis, *Digital Signal Processing (4th Edition)*, 4th ed. Prentice Hall, Apr. 2006.

[21] S. Sesia, I. Toufik, and M. Baker, *LTE, The UMTS Long Term Evolution: From Theory to Practice*. Wiley Publishing, 2009.

[22] "LTE; evolved universal terrestrial radio access (E-UTRA); relay radio transmission and reception," 3GPP TS 36.16 version 11.4.0 Release 11, Tech. Rep., Apr. 2015.

[23] "Universal mobile telecommunications system (UMTS); selection procedures for the choice of radio transmission technologies of the UMTS," UMTS 30.03 TR 101 112, V3.1.0, Tech. Rep., Apr. 1998.